

Experimental Investigation of Soil Thermal Conductivity Over a Wide Temperature Range

Ivan V. Nikolaev · Wey H. Leong · Marc A. Rosen

Received: 7 August 2011 / Accepted: 6 May 2013 / Published online: 2 June 2013
© Springer Science+Business Media New York 2013

Abstract The results are reported of an experimental investigation of the soil thermal conductivity over a wide temperature range, for various water contents and two soil types. The results are particularly important in predictions of underground heat transfer, which require a quantitative understanding of the coupled dependence of the soil thermal conductivity on texture, temperature, and water content. In the research, comprehensive sets of thermal conductivity for Ottawa sand (coarse soil) and Richmond Hill fine sandy loam (medium soil) are experimentally obtained using the guarded hot-plate method, for temperatures ranging from 2 °C to 92 °C and water contents varying from complete dryness to full saturation. For both soils, the thermal conductivity is observed to vary in three stages with respect to increasing water content: a very minor increase as water content increases to the permanent wilting point, a steep increase as water content further increases to field capacity, and a minor increase (for temperatures less than 72 °C) or decrease for (temperatures greater than 72 °C) when the field capacity is exceeded. Then, on the basis of gathered datasets, a similar $Ke(S_r, T)$ form of the soil thermal conductivity model by Tarnawski et al. is used to empirically fit the data. The resulted correlations fit the data well with their overall root-relative-mean-square percentage errors of 4.7 % and 6.1 % for Ottawa sand and

I. V. Nikolaev (✉) · W. H. Leong
Department of Mechanical and Industrial Engineering, Ryerson University, 350 Victoria Street,
Toronto, ON M5B 2K3, Canada
e-mail: i.nikolaev@utoronto.ca

W. H. Leong
e-mail: weyleong@ryerson.ca

M. A. Rosen
Faculty of Engineering and Applied Science, University of Ontario Institute of Technology,
2000 Simcoe Street North, Oshawa, ON L1H 7K4, Canada
e-mail: marc.rosen@uoit.ca

Richmond Hill fine sandy loam, respectively, and are suitable for most engineering applications.

Keywords Guarded hot-plate method · Soil thermal conductivity · Thermal-conductivity modeling · Underground heat transfer

1 Introduction

Accurate soil thermal properties are necessary for numerous engineering, environmental, and agronomical applications. A property often of interest is the effective thermal conductivity, λ , since it reflects the ability of soil to conduct heat. This makes thermal conductivity an important parameter in solving problems of ground waste disposal, geothermal energy extraction, enhanced oil recovery, ground thermal storage, thermal soil remediation, behavior under forest fires, and climate tuning of buildings to specific environments, to name a few. Not surprisingly, numerous attempts have been made to develop advanced analytical techniques to predict quickly the thermal conductivity of soils and, although these approaches have evolved significantly over the past several decades, none is capable of precise estimation. This is mainly because of the complexity of the model formulation, since the thermal conductivity of soil depends on numerous interconnected parameters which are difficult to incorporate into a single model. Also, reliable experimental data are required to properly calibrate and verify a model, and such data are not widely available.

In general, thermal-conductivity models of soils are classified as empirical or theoretical. The theoretical modeling involves an approximate analytical reconstruction of the actual soil structure, based on its properties, and as such, is very challenging due to the dependence on a wide variety of parameters, including mineral composition, particle shape and size distribution, temperature, dry density, porosity, water content, etc. Some of these parameters are hard to measure precisely, and it is difficult to incorporate all of them into a single universal model. Moreover, analytical models normally involve empirical coefficients which also cannot be estimated precisely [1].

In comparison, empirical modeling is based purely on the numerical and mathematical analyses of experimental data. Empirical correlations are much easier to use and incorporate in numerical algorithms, but are primarily dependent on the accuracy of the experimental data [2]. Numerous correlations for soil thermal conductivity have been proposed. Among others, Kersten [3], Gemant [4], Johansen [5], de Vries [6], Van Rooyen and Winterkorn [7], Cote and Konrad [8], Tarnawski and Leong [9], and Tarnawski and Gori [10] have developed correlations that vary in complexity. Each of these correlations is limited to a certain type of soil as well as specific conditions. Kersten [3] based his correlations on empirical data he collected. He produced expressions for the thermal conductivity of frozen and unfrozen silt and sandy soils as a function of water content and dry density. However, as shown by Farouki [11], Kersten's correlation is accurate only for frozen soils with saturations up to 90 %. Also, for a very low degree of saturation down to dry state, the correlation produces negative thermal conductivity values. Gemant's correlation [4] assumes an idealized geometrical model of soil particles with point contacts. The soil thermal conductivity is derived

as a function of the dry bulk density (ratio of dry soil mass to dry soil volume), water content, apex water (i.e., water collected around the contact points), water absorbed as a film around the soil particles, and thermal conductivities of water and solids. However, Gemant's correlation gives a reasonable estimate for only unfrozen sandy soils. Johansen's correlation [5] presents the soil thermal conductivity as a function of the degree of saturation, and is suitable for both coarse and fine grained soils in the frozen and unfrozen states. However, accurate results are predicted for water content up to 20 %. The de Vries model [6], based on the assumption that soil is composed of two phases, considers solid uniform ellipsoidal particles within a fluid. The method represents the thermal conductivity as a function of the solid volume fraction and the thermal conductivities of the solid and fluid phases. However, its results are reasonable only for unfrozen coarse soils with saturations of 10 % to 20 %. The correlation developed by Van Rooyen and Winterkorn [7] is based on data collected for sands and gravels. The thermal conductivity is given as a function of the degree of saturation, dry density, mineral type, and particle shape. The Van Rooyen and Winterkorn correlation is limited to unfrozen sands and gravels with saturation levels between 1.5 % and 10 %. A common deficiency in all these correlations is a very narrow range of water content.

Another major problem with analytical modeling is a lack of comprehensive and accurate experimental research for proper verification and calibration, especially for low to intermediate water contents and temperatures above 50 °C. Even the most recent and advanced analytical and numerical studies are verified on the basis of limited experimental data. For instance, using the heated probe method, Sepaskhah and Boersma [12] provide thermal-conductivity data for loamy sand, loam, and silty clay loam textures, but at only two moderate temperatures (25 °C and 45 °C) and a limited range of water content (with some soil texture, porosity, and bulk density data being misprinted). Another well-referenced experimental study by Campbell et al. [13] is more extensive and involves nine soils, covering three textural groups: coarse soils (L-soil, Royal, Volkmar), medium soils (Palouse-A, Salkum, Mokins, Walla Walla), and fine soils (Palouse-B, Boulder creek). The thermal conductivity was measured using the heated probe method for a temperature range of 30 °C to 90 °C, at 20 °C intervals. However, the data are reliable only for lower temperatures (30 °C and 50 °C), since the data vary somewhat erratically with water content for temperatures of 70 °C and 90 °C. The thermal study conducted by Black et al. [14] for Ottawa sand was based on the heated dual-probe technique as well as a guarded hot-plate (GHP) apparatus. However, the study does not mention the temperature range over which the measurements were taken. Moreover, the thermal-conductivity measurements for low water contents are significantly scattered and thus are of doubtful validity. The reason is probably moisture migration around the probes, which also resulted in the thermal conductivity measured by a heated probe being on average lower than the GHP measurements. One of the most reliable studies was conducted recently by Hiraiwa and Kasubuchi [15] on the basis of dual-heated probes and involved thermal-conductivity measurements of clay loam and light clay soil textures for the temperature range of 5 °C to 75 °C, at 10 °C intervals. However, the temperature range is not extensive enough for comprehensive verification of high- or low-temperature models. A common deficiency in all these studies is the absence of detailed information regarding particle size distribution and

mineralogical composition of the soil samples, which are crucial for refining the model. The experiments were done over limited low- to mid-temperature ranges, in many cases exhibiting a questionable accuracy. Despite limitations, these datasets are commonly used for theoretical and numerical modeling.

The objective of this research is to aid the development of accurate high-temperature models of soil thermal conductivity by establishing comprehensive sets of experimental data and corresponding models for two soils with established physical and mineralogical properties over a wide temperature range (2 °C to 92 °C). First, an extensive experimental thermal-conductivity study is conducted for two soils of different textures and particle size distribution: Ottawa sand (coarse soil) and Richmond Hill fine sandy loam (medium soil). Then, a similar $Ke(S_r, T)$ form of the soil thermal-conductivity model of Tarnawski et al. [16] is used to correlate between the model and the experimental datasets.

2 Experimental Technique and Procedures

2.1 Preparation of Soil Samples

Soil thermal properties are strongly influenced by the soil volumetric water content as well as by the volume fraction of solid and air. Since air is a poor thermal conductor, it reduces the effectiveness of the partially saturated soil in conducting heat; and while the solid phase has the highest conductivity, it is the variability of moisture within the sample that most influences the thermal conductivity. Hence, a successful experimental measurement of soil thermal conductivity requires a careful and reliable sample preparation technique. Dry soil properties such as dry bulk density and soil particle density have to be precisely measured since, without them, the thermal data are much less meaningful. Then water is added to achieve the desired water content according to the procedure described below.

The specimen preparation procedure is based on that first introduced by Holton et al. [17]. First, the soil samples are dried in an oven at 105 °C for 24 h. The dry-bulk density is then determined by

$$\rho_{db} = \frac{M_{ds}}{V_c} \quad (1)$$

where M_{ds} is the mass of the dry soil which is hard-packed into a sample container of volume V_c . The porosity (void fraction) of the soil samples is calculated by

$$\phi = 1 - \frac{\rho_{db}}{\rho_s} \quad (2)$$

where ρ_s is the density of soil solid particles. Then, to obtain a specific volumetric water content, θ_w , the following equation is used to determine the required volume V_w or mass M_w of water to be added to the dry soil:

$$V_w = V_c \theta_w \quad (3)$$

$$M_w = V_c \theta_w \rho_w \quad (4)$$

The dry sample is hand mixed in a sealed ziploc bag with the required amount of water. To achieve a more uniform moisture distribution, the sample is heated in cycles in a microwave oven and eventually left for 48 h in a constant-temperature environment. Consequently, the sample is hard-packed into an experimental container, made from electroplated 0.20 mm thick mild steel, and covered by an overlapping sliding lid. The containers are sealed with a non-hardening, high-temperature resistant sealant for pressures up to 34.5 MPa. The containers are then weighed and left for 24 h for the sealant to cure. Finally, the weight and the thickness of the filled container are measured again and it is ready for the experiment. The diameter and thickness of soil layer are about 150 mm and 20 mm, respectively. After the experiment the container is weighed again for making sure of no loss of moisture, and then the sealant is removed and the soil is dried in the oven for 24 h. The mass of dry soil is then determined and divided by the volume of the container to get the dry bulk density of the soil. The volumetric water content, θ_w , can also be re-evaluated through the mass difference between before and after drying.

2.2 Properties and Composition of Experimental Soils

Samples of two types of soils, namely, Ottawa sand and Richmond Hill fine sandy loam, are used in this study. The Ottawa sand is a natural silica coarse sand with 99 % quartz content, a particle density $\rho_s = 2650 \text{ kg} \cdot \text{m}^{-3}$, a dry bulk density $\rho_{\text{db}} = 1680 \text{ kg} \cdot \text{m}^{-3}$ (at well-compacted condition), a porosity $\phi = 0.366$, and particles with diameters variation from 0.59 mm to 0.84 mm [18]. The Ottawa sand is chosen because it has been studied extensively at low temperatures [18–20] and thus can be used as a reference material for verification of experimental results. The Richmond Hill soil is grayish-brown in color when dry, and has a fine sandy loam texture. The soil has been extracted from a site in the town of Richmond Hill, Ontario, at the northeast corner of Bayview Avenue and Elgin Mills Road from three pits 50 cm to 60 cm deep and approximately 50 m apart from each other. The samples were extracted below the top fertile layer (25 cm to 30 cm) and hence are not influenced by biological activity nor do they contain organic matter. The original soil comprises about 13 % to 15 % rock/gravel fragments, which are 3 mm in average diameter, however the soil has been sieved through a 2 mm mesh screen to remove them. The sieved soil for the experiment has the following composition: sand mass fraction $m_{\text{sa}} \approx 0.523$, silt mass fraction $m_{\text{si}} \approx 0.322$, and clay mass fraction $m_{\text{cl}} \approx 0.155$. The mass fractions of the particle size distribution for Richmond Hill fine sandy loam can be found in Table 1. The average particle density of Richmond Hill soil is around $2650 \text{ kg} \cdot \text{m}^{-3}$ (which is typical for most North American soils), the dry bulk density is $\rho_{\text{db}} = 1137 \text{ kg} \cdot \text{m}^{-3}$ (at well compacted condition), and the porosity is calculated to be $\phi = 0.571$, which is typical for its textural class. According to Bristow [21], the quartz content in a soil strongly influences the thermal conductivity of soil solids, because quartz has a much higher thermal conductivity than other minerals. The complete mineral composition (as tabulated in Table 1 with an absolute error of 2 mass% to 3 mass% of the soil

Table 1 Mass fractions of particle size distribution and mineral composition for Richmond Hill fine sandy loam

Name of particle	Particle size (μm)	Fraction (mass%)	Mineral	Fraction (mass%)
Very coarse sand	1000–2000	2.8	Quartz	33
Coarse sand	500–1000	5.4	K-feldspar	7
Medium sand	250–500	10.3	Plagioclase	20
Fine sand	100–250	19.9	Actinolite	2
Very fine sand	53–100	13.9	Calcite	29
Silt	2–53	32.2	Chlorite	6
Clay	<2	15.5	Clay	3

Table 2 Permanent wilting point, field capacity, and full saturation points of two tested soils

Volumetric water content ($\text{m}^3 \cdot \text{m}^{-3}$)	Ottawa sand	Richmond Hill soil
θ_{PWP}	0.092	0.143
θ_{FC}	0.183	0.290
θ_{FS}	0.366	0.571

is obtained by combined use of the X-ray diffraction (XRD) and X-ray fluorescence (XRF) techniques. Using the geometric mean model, i.e., $\lambda_s = \lambda_{\text{qtz}}^{\Theta_{\text{qtz}}} \lambda_{\text{o-min}}^{1-\Theta_{\text{qtz}}}$ with $\lambda_{\text{qtz}} = 7.7 \text{ W} \cdot \text{m}^{-1} \cdot \text{K}^{-1}$ and $\lambda_{\text{o-min}} = 2.13 \text{ W} \cdot \text{m}^{-1} \cdot \text{K}^{-1}$ at 20°C [22], the thermal conductivity of soil solids for Richmond Hill fine sandy loam is estimated to be $\lambda_s = 3.26 \text{ W} \cdot \text{m}^{-1} \cdot \text{K}^{-1}$ for $\Theta_q = 0.33 \text{ m}^3$ of quartz per m^3 of soil solids. The empirical correlations for λ_s and Θ_q developed by Tarnawski et al. [22], based on measured quartz contents of 40 Canadian soils, give $\lambda_s = 3.30 \text{ W} \cdot \text{m}^{-1} \cdot \text{K}^{-1}$ and $\Theta_q = 0.35 \text{ m}^3$ of quartz per m^3 of soil solids, which are about 1.4 % and 6.1 % differences, respectively.

The permanent wilting point, θ_{PWP} , and the soil's field capacity, θ_{FC} , are then estimated on the basis of physical properties. In particular, a useful rule of thumb is to estimate θ_{FC} as $\phi/2$, and θ_{PWP} as $\theta_{\text{FC}}/2$. Banin and Amiel [23] and Dahiya et al. [24] have demonstrated that the assumed ratios of

$$\frac{\theta_{\text{FC}}}{\phi} = \frac{1}{2} \quad (5)$$

and

$$\frac{\theta_{\text{PWP}}}{\phi} = \frac{1}{4} \quad (6)$$

are good approximations, based on measured correlations on many soils. Table 2 shows the volumetric water contents at the permanent wilting point, field capacity, and full saturation for Ottawa sand and Richmond Hill fine sandy loam.

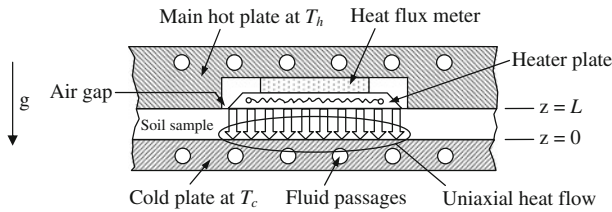


Fig. 1 General illustration of GHP apparatus

3 Measurement of Thermal Conductivity

The effective soil thermal conductivity is measured by a steady-state technique called the GHP method, which involves a monitored uniaxial heat flux through a specimen fixed between parallel plates (Fig. 1). The principle of this technique is to generate a steady known heat flux that flows unidirectionally through a specimen between the planes of hot and cold plates. The hot plate consists of a main copper plate (178 mm × 178 mm × 19 mm) and a copper heater plate (metering device) embedded in a recess (78 mm × 78 mm × 6.4 mm). The main plate forms a guard around the metering device embedded in the center separated by an air gap of 0.80 mm, which acts as a thermal barrier. The cold plate consists of a copper plate (178 mm × 178 mm × 13 mm), which is thinner than the hot plate because it does not contain any embedded metering device. The hot and cold plates are maintained at different temperatures by two streams of circulating fluid through passages drilled in the plates (see Fig. 1), each uniform to within 0.03 °C. Details on the design, operation, and measurement principles of the GHP apparatus are presented in Reid et al. [25] and Reid [26].

In order to capture the complete trend of thermal-conductivity variation with water content, the following eleven to twelve experimental points of volumetric water content are considered: one point at dry condition ($\theta_w = 0$), two points within the barely moist range ($0 < \theta_w < \theta_{PWP}$), five points within the moderately moist range ($\theta_{PWP} < \theta_w < \theta_{FC}$), two or three points within the highly moist range ($\theta_{FC} < \theta_w < \theta_{FS}$), and one point at fully saturated condition ($\theta_w = \theta_{FS} = \phi$). Based on these volumetric water contents, the soil samples were prepared accordingly.

The thermal conductivity is obtained for a temperature range of 2 °C to 92 °C, at 10 °C intervals, with $\Delta T = 4$ °C between the hot and cold plates, and for water contents from completely dry to fully saturated conditions. The ΔT of 4 °C is found to be an optimum temperature difference for maximizing the sensitivity of measuring equipment and minimizing the temperature gradient across the specific thickness of present soil samples through a series of preliminary tests. The resulting temperature gradient for the entire study is about $170 \text{ K} \cdot \text{m}^{-1}$, which gives a range of heat flux through the soil samples ranging from about $38 \text{ W} \cdot \text{m}^{-2}$ to $765 \text{ W} \cdot \text{m}^{-2}$. The overall error of each measurement is a combination of quantifiable errors from various sources, such as temperature non-uniformity of apparatus, calibration, signal conditioning, data acquisition, and data reduction. The overall experimental uncertainty associated with the 95 % confidence level, $U_{0.95}$, of all thermal-conductivity measurements is determined to be 3.0 %, which is obtained by combining both the precision and bias errors through the root-sum-square method [27]. There may also be effects due to non-

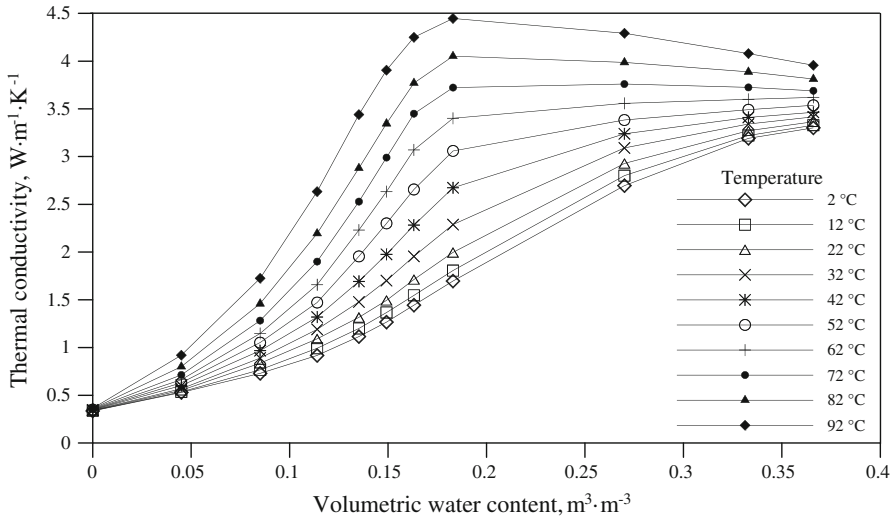


Fig. 2 Variation in thermal conductivity of Ottawa sand with volumetric water content and temperature

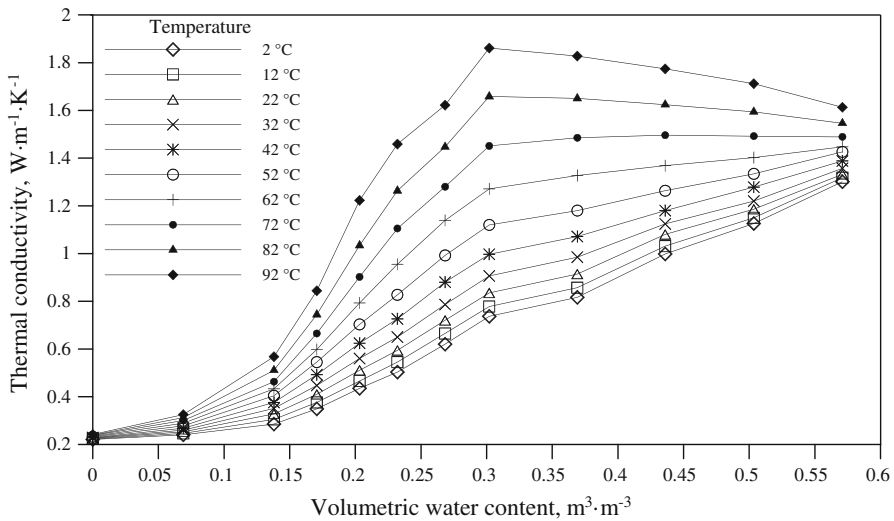


Fig. 3 Variation in thermal conductivity of Richmond Hill fine sandy loam with volumetric water content and temperature

quantifiable parameters, such as moisture re-distribution in soil layer (due to gravity and thermal gradient) and homogeneity of soil sample.

4 Discussion of Experimental Results

The variations in the thermal conductivity of Ottawa sand and Richmond Hill soil with volumetric water content for each temperature investigated are plotted in Figs. 2 and 3, respectively (for tabulated data, please refer to the Appendix Tables 5 and 6).

The straight lines joining the data points are only for demonstration purposes and may not be the true trends. The effects of temperature and water content are clearly visible on the graphs. In particular, in both cases the thermal conductivity increases in three stages with respect to increasing water content. At very low water contents up to the permanent wilting point, the thermal conductivity of soils increases slowly, since the water just coats the soil particles and the voids between the soil particles are not filled with water. At the permanent wilting point, the particles are fully coated with water, and as the water content further increases, the water fills the gaps between the soil particles. This results in the rapid increase of the heat flow between the particles caused by a rapidly increasing thermal conductivity. The rapid increase is even more prominent for high temperatures, such as those greater than 62 °C, resulting in a peak thermal conductivity greater than the one at full saturation, which may be a result of water vapor migration through air passages in the soils [28]. However, when the field capacity is exceeded, the voids are mostly filled, and a further increase in water content does not appreciably increase the heat flow between the particles. Thus, the thermal conductivity increases slightly after that point. Moreover, as the temperature exceeds approximately 65 °C to 70 °C for both soils, the thermal conductivity slowly decreases as the volumetric water content exceeds $\sim 0.2 \text{ m}^3 \cdot \text{m}^{-3}$ to $0.25 \text{ m}^3 \cdot \text{m}^{-3}$ and $\sim 0.3 \text{ m}^3 \cdot \text{m}^{-3}$ to $0.37 \text{ m}^3 \cdot \text{m}^{-3}$ for Ottawa sand and Richmond Hill fine sandy loam, respectively. This observation may be explained by the formation of small air pockets, which are completely surrounded by soil particles and water; water vapor stays within the air pockets and does not easily migrate, leading to a reduction in heat transfer due to limited mass transfer.

Ottawa sand (a coarse textured soil) has higher thermal conductivities than Richmond Hill fine sandy loam (a medium textured soil) by an average of 1.5 to 2.6 times, corresponding from dry to full saturation, for all experimental temperatures. It can also be observed from Figs. 2 and 3 that the thermal conductivities for 2 °C, 12 °C, and 22 °C (maybe up to 30 °C) are relatively similar; however, for higher temperatures (especially greater than 40 °C), the effect of temperature on the thermal conductivity is more obvious and causes the curves to shift further upward. This may suggest that the heat transfer in the low-temperature range (2 °C to 30 °C) is dominated by conduction through the moist soils with very limited extent due to vapor migration. When the temperature is high enough (such as greater than 40 °C), the heat transfer due to vapor migration becomes noticeable, resulting in an apparent or effective thermal conductivity which may be greater than the thermal conductivity due to pure heat conduction alone in the moist soils.

For moderately moist soils ($\theta_{\text{PWP}} < \theta_w \leq \theta_{\text{FC}}$) at high temperatures, vapor migration (i.e., mass transfer) plays a very significant role in heat transfer, effecting a rapid increase in the thermal conductivity. As shown in Figs. 4 and 5, the rapid increase in the thermal conductivity for a volumetric water content θ_w between θ_{PWP} and θ_{FC} , which corresponds to the degree of saturation S_r between 0.25 and 0.50, is the most significant, reaching as high as 200 % at 92 °C with respect to the thermal conductivity at 2 °C. A change of slope can also be observed at temperatures between 32 °C and 42 °C in Figs. 4 and 5, which indicates that vapor migration becomes more significant. In fact, for very high temperatures of 82 °C and 92 °C, the peak thermal conductivity near the field capacity is even greater than the one at full saturation. For example, the

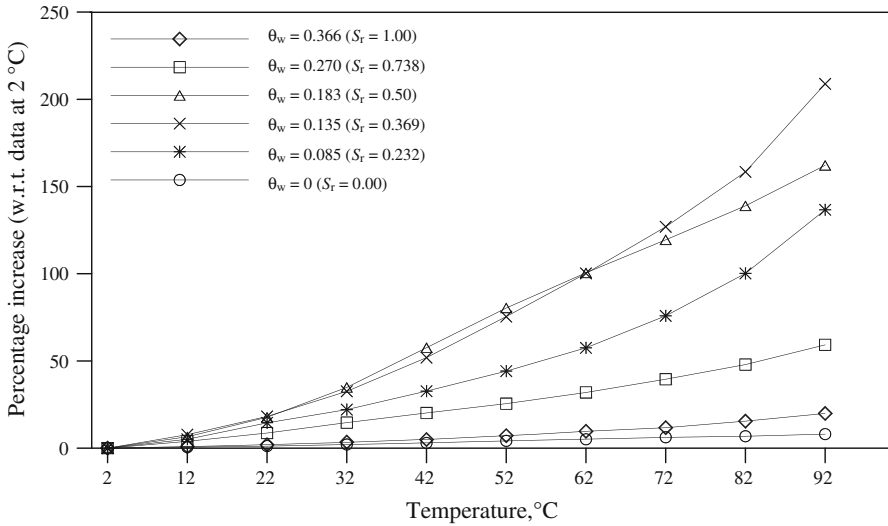


Fig. 4 Percentage increase of thermal conductivity of Ottawa sand with respect to the thermal conductivities at 2 °C for various volumetric water contents

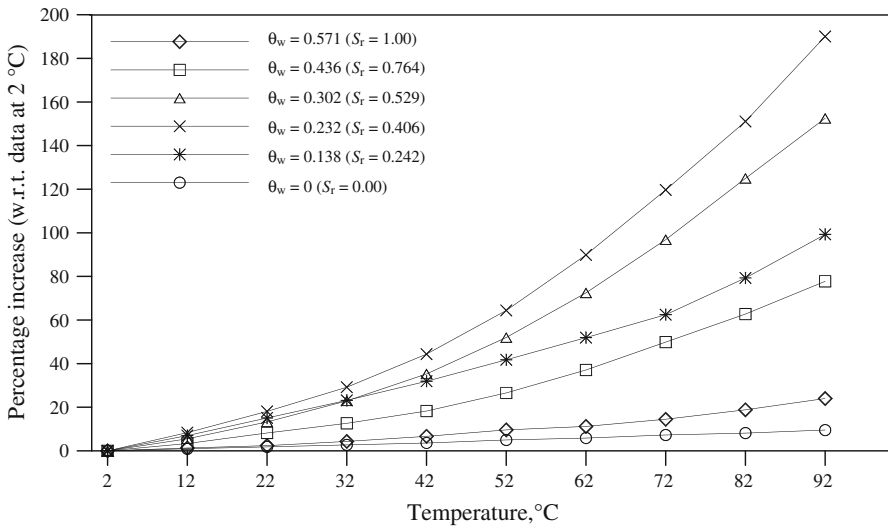


Fig. 5 Percentage increase of thermal conductivity of Richmond Hill fine sandy loam with respect to the thermal conductivities at 2 °C for various volumetric water contents

peak thermal conductivities of Ottawa sand and Richmond Hill fine sandy loam at 92 °C are $4.45 \text{ W} \cdot \text{m}^{-1} \cdot \text{K}^{-1}$ and $1.86 \text{ W} \cdot \text{m}^{-1} \cdot \text{K}^{-1}$, respectively, which are about 12 and 8 times greater than their respective thermal conductivities at dry condition or about 1.12 and 1.15 times greater than their respective thermal conductivities at full saturation. At dry and saturated conditions, where no vapor migration occurs, the thermal conductivity only increases about 10 % and 20 %, respectively, over the temperature range of 2 °C to 92 °C. At near dryness and near saturation conditions,

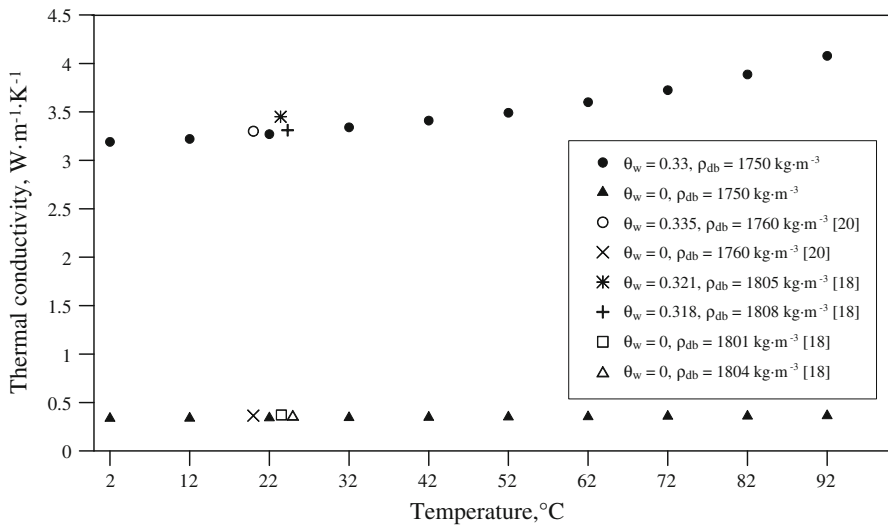


Fig. 6 Experimental and published thermal-conductivity values of Ottawa sand

such as $S_r \approx 0.25$ and 0.75 , respectively, the effect of vapor migration is relatively moderate and the increase in thermal conductivity over the temperature range is about 100 % to 140 % and 60 % to 80 %, respectively.

4.1 Verification of Results

In order to verify the accuracy of the GHP apparatus as well as the sample preparation methodology, preliminary tests were conducted to obtain thermal conductivities of Ottawa sand at 20 °C to 25 °C for 0 and $0.339 \text{ m}^{-3} \cdot \text{m}^{-3}$ water contents and the results were compared to several published values. The results are presented in Fig. 6 and are in excellent agreement with results of Bligh and Smith [18] and Moench and Evans [20]. Both sets of results exhibit a strong dependence of the soil thermal conductivity on water content. The current result for the saturated sample at 22 °C has a maximum discrepancy of 5.2 % lower than the reference data. This discrepancy may be attributed to as much as 3.1 % higher dry-bulk density in [18] ($1750 \text{ kg} \cdot \text{m}^{-3}$ vs $1805 \text{ kg} \cdot \text{m}^{-3}$) and also a 4.0 % overall uncertainty ($U_{0.95}$) of thermal conductivity measurement at $\Delta T = 2^\circ\text{C}$.

In the case of a dry Ottawa sand, the thermal conductivity remains almost constant over the entire temperature range, increasing very gradually in a linear manner from $0.33 \text{ W} \cdot \text{m}^{-1} \cdot \text{K}^{-1}$ to $0.36 \text{ W} \cdot \text{m}^{-1} \cdot \text{K}^{-1}$ within the 2 °C to 92 °C temperature range, which is about 10 % increase and is less than the percentage increase (28 % increase) in the thermal conductivity of air over the same temperature range. This increasing trend agrees well with the observation of Tarnawski et al. [29]. They explain that the air acts as a very effective thermal insulator around the quartz sand particles; as a result, a diminutive increase of the thermal conductivity with temperature is driven by increasing the thermal conductivity of air, overshadowing the decreasing trend of quartz's thermal conductivity with temperature.

For the case of a saturated Ottawa sand, the increase is noticeable and nonlinear, varying from around $3.19 \text{ W} \cdot \text{m}^{-1} \cdot \text{K}^{-1}$ to $4.08 \text{ W} \cdot \text{m}^{-1} \cdot \text{K}^{-1}$ within the 2°C to 92°C temperature range, which is about 28 % increase. This increase is greater than the percentage increase (20 % increase) in the thermal conductivity of water over the same temperature range. However, this increasing trend does not agree with the observation of Tarnawski et al. [30], who using a transient thermal-conductivity probe measured a slight decreasing trend of the thermal conductivity of saturated Ottawa sand with increasing temperature. This is due to the decreasing trend of quartz’s thermal conductivity within the 2°C to 92°C temperature range, which is about a 23 % decrease [30]. In order to investigate the different observations, the following steady-state balance equations of fluid mass and energy together with the Brinkman equation [31], which includes the effects of Darcian, thermo-osmosis, and Boussinesq buoyant flows [32], respectively, are employed:

$$\nabla \cdot \vec{u} = 0 \tag{7}$$

$$\nabla \cdot (\lambda_{\text{sat}} \nabla T) - \rho_w c_w \vec{u} \cdot \nabla T = 0 \tag{8}$$

$$-\nabla p - \frac{\mu_w}{\kappa} k_T \nabla T - \rho_w g \beta_w (T_c - T) \nabla z + \mu_w \nabla^2 \vec{u} = \frac{\mu_w}{\kappa} \vec{u} \tag{9}$$

where $\vec{u} = u\hat{i} + v\hat{j} + w\hat{k}$, is the volumetric average velocity or volumetric water flux vector ($\text{m} \cdot \text{s}^{-1}$); T is the temperature (K); T_c is the cold-plate temperature and is used as a reference temperature; p is the interstitial average pressure (Pa); z is the elevation (m); ρ_w is the density of water ($\text{kg} \cdot \text{m}^{-3}$); c_w is the specific heat of water ($\text{J} \cdot \text{kg}^{-1} \cdot \text{K}^{-1}$); μ_w is the dynamic viscosity of water ($\text{kg} \cdot \text{m}^{-1} \cdot \text{s}^{-1}$); β_w is the volumetric expansion coefficient of water (K^{-1}); κ is the intrinsic permeability of saturated soil (m^2); k_T is the thermo-osmotic permeability of saturated soil ($\text{m}^2 \cdot \text{K}^{-1} \cdot \text{s}^{-1}$); λ_{sat} is the thermal conductivity of saturated soil ($\text{W} \cdot \text{m}^{-1} \cdot \text{K}^{-1}$); and g is the gravitational acceleration ($\text{m} \cdot \text{s}^{-2}$).

The boundary condition for the velocity field is

$$\vec{u} = 0 \text{ (all walls have no-slip conditions)} \tag{10}$$

The boundary conditions for the temperature field are

$$T = T_h \text{ (prescribed high temperature at } z = L, \text{ i.e., top surface)} \tag{11}$$

$$T = T_c \text{ (prescribed low temperature at } z = 0, \text{ i.e., bottom surface)} \tag{12}$$

$$\hat{n} \nabla T = 0 \text{ (insulated at vertical side walls)} \tag{13}$$

The fully-coupled system of Eqs. 7 to 9 can be numerically solved for the pressure (p), temperature (T), and fluid velocity (u , v , and w) with the boundary conditions (Eqs. 10 to 13).

The saturated hydraulic conductivity of Ottawa sand was measured to be $K_h = 5.71 \times 10^{-3} \text{ m} \cdot \text{s}^{-1}$ at 24°C , using the falling-head method. The intrinsic permeability is related to the saturated hydraulic conductivity.

$$\kappa = K_h \frac{\mu}{\rho g} \quad (14)$$

Therefore, the value of the intrinsic permeability of Ottawa sand is obtained to be $\kappa = 5.28 \times 10^{-10} \text{ m}^2$. However, there is no equipment which is accessible by the authors to measure the thermo-osmotic permeability of Ottawa sand. Also, there are no data available for the thermo-osmotic permeability of sand in the open literature. Nonetheless, there are few experimental data for compacted clay. The range for the thermo-osmotic permeability of compacted clay is between $10^{-14} \text{ m}^2 \cdot \text{K}^{-1} \cdot \text{s}^{-1}$ and $10^{-10} \text{ m}^2 \cdot \text{K}^{-1} \cdot \text{s}^{-1}$ [32,33]. Sorel [32] also gives the range of the saturated hydraulic conductivity of compacted clay to be between $10^{-14} \text{ m} \cdot \text{s}^{-1}$ and $10^{-11} \text{ m} \cdot \text{s}^{-1}$. The values of the thermo-osmotic permeability and saturated hydraulic conductivity seem to have about the same order of magnitude. Therefore, it is deduced that the thermo-osmotic permeability of Ottawa sand is in the range of $10^{-7} \text{ m}^2 \cdot \text{K}^{-1} \cdot \text{s}^{-1}$ to $10^{-3} \text{ m}^2 \cdot \text{K}^{-1} \cdot \text{s}^{-1}$, assuming that the measured saturated hydraulic conductivity is at the high end of the range. Five cases of the mean temperature ($T_m = (T_h + T_c) / 2 = (25, 40, 50, 60, \text{ and } 70) \text{ }^\circ\text{C}$) were simulated using COMSOL Multiphysics [34], due to the known λ_{sat} values for these temperatures from Tarnawski et al. [30]. According to Tarnawski et al., their transient thermal conductivity probe was powered for only 120 s for each measurement. Over the short duration of measurement, the thermal osmosis is practically non-existent. Therefore, their measured thermal conductivities can be considered as λ_{sat} and are given in Table 3, which are adjusted by interpolation to match with the present porosity of $0.339 \text{ m}^3 \cdot \text{m}^{-3}$. Figure 7 shows a finite element mesh of the simulated soil layer as a porous medium in a sample container. The fluid properties used in the simulations are evaluated at T_m and are treated as constants (see Table 3).

Due to the unknown value of the thermo-osmotic permeability, a preliminary study was conducted to obtain a probable value of the thermo-osmotic permeability of Ottawa sand by varying its value from $10^{-7} \text{ m}^2 \cdot \text{K}^{-1} \cdot \text{s}^{-1}$ to $10^{-3} \text{ m}^2 \cdot \text{K}^{-1} \cdot \text{s}^{-1}$ for the case of $T_m = 25 \text{ }^\circ\text{C}$. It was found that in the confined space of the container, the Darcian (due to the developed reverse pressure as a result of the thermo-osmosis flow) and the heating-from-above buoyant flows almost counteract the thermo-osmosis flow. The fluid velocity and, hence, the convective heat flux from the hot plate to the cold plate increase with the thermo-osmotic permeability. After many trials, the value of $k_T = 1.7 \times 10^{-5} \text{ m}^2 \cdot \text{K}^{-1} \cdot \text{s}^{-1}$ was finally found to produce a satisfactory result. The same value of the thermo-osmotic permeability was then used for the other cases of T_m . As a result, the total heat flux (conduction + convection) from each case was obtained and then the effective thermal conductivity of the soil layer was calculated as follows:

$$\lambda_{\text{eff}} = \frac{q_T}{\Delta T / L} \quad (15)$$

where q_T is the total heat flux ($\text{W} \cdot \text{m}^{-2}$), $\Delta T = T_h - T_c = 2 \text{ K}$, and $L = 0.020 \text{ m}$. The effective thermal conductivities are tabulated in Table 3 and they are within 1 % difference with respect to the present experimental data. Therefore, it can be concluded that the increasing trend of the measured thermal conductivity of saturated Ottawa

Table 3 Property values and simulated results of effective thermal conductivity of a saturated Ottawa sand layer

T_m (°C)	T_h (°C)	T_c (°C)	c_w (J · kg ⁻¹ · K ⁻¹)	ρ_w (kg · m ⁻³)	μ_w (N · s · m ⁻²)	β_w (K ⁻¹)	λ_{sat} (W · m ⁻¹ · K ⁻¹)	λ_{GHP} (W · m ⁻¹ · K ⁻¹)	λ_{eff} (W · m ⁻¹ · K ⁻¹)	% diff.
25	26	24	4179	997	8.87×10^{-4}	2.56×10^{-4}	3.21	3.30	3.32	0.61
40	41	39	4179	992	6.53×10^{-4}	3.90×10^{-4}	3.16	3.39	3.40	0.29
50	51	49	4181	988	5.47×10^{-4}	4.63×10^{-4}	3.14	3.48	3.49	0.29
60	61	59	4185	983	4.67×10^{-4}	5.27×10^{-4}	3.11	3.58	3.57	0.28
70	71	69	4190	978	4.05×10^{-4}	5.85×10^{-4}	3.06	3.71	3.68	0.81

$\kappa = 5.28 \times 10^{-10} \text{ m}^2$ and $k_T = 1.7 \times 10^{-5} \text{ m}^2 \cdot \text{K}^{-1} \cdot \text{s}^{-1}$. λ_{sat} 's are based on Tamawski et al. [30]. λ_{GHP} 's are based on present experiment, which are adjusted to T_m . λ_{eff} 's are calculated using Eq. 15. The percent differences are calculated as $|\lambda_{eff} - \lambda_{GHP}| / \lambda_{GHP} \times 100$

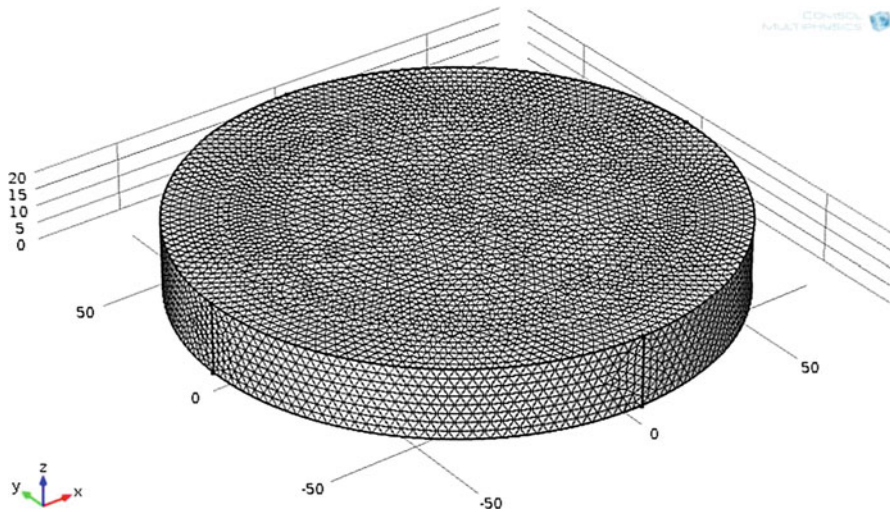


Fig. 7 Finite element mesh of the simulated soil layer in a sample container

sand with temperature is an artifact of the GHP apparatus which is operated under steady-state conditions with an established temperature gradient to drive liquid water migration.

Thus, the GHP apparatus is capable of producing results which are in excellent agreement with reference data, except for the case of saturated Ottawa sand. Although the GHP apparatus is unable to measure the thermal conductivity of the saturated Ottawa sand for pure heat conduction only, it is capable of measuring the effective thermal conductivity of the soil with the water migration driven by the temperature gradient (also called thermal osmosis).

4.2 Empirical Modeling of Soil Thermal Conductivity

From the measured data, it is evident that the behavior of the soil thermal conductivity is strongly dependent on the temperature and water content. An increase in either leads to an increase in the soil thermal conductivity. An empirical correlation model of soil thermal conductivity by Tarnawski et al. [16], as a function of both temperature and water content, is originally considered in this research. However, it is not fitted satisfactorily to the present experimental datasets. Therefore, a number of similar functions were tried and the following function is found to be very satisfactory for fitting the present experimental Kersten (Ke) numbers.

$$Ke(S_r, T) = \frac{a_1 + a_2 S_r + a_3 S_r^2 + a_4 S_r^3 + a_5 T}{1 + a_6 S_r + a_7 S_r^2 + a_8 T + a_9 T^2 + a_{10} T^3} \quad (16)$$

where $S_r = \theta_w / \phi$ (the degree of saturation) and T is in $^{\circ}\text{C}$.

Table 4 Correlation coefficients of Eq. 16 for Ottawa sand and Richmond Hill fine sandy loam

Correlation coefficient	Ottawa sand	Richmond Hill fine sandy loam
a_1	-6.7346×10^{-3}	-6.6775×10^{-3}
a_2	0.601415	0.214586
a_3	-1.53135	-0.303667
a_4	2.38584	1.46713
a_5	2.1202×10^{-4}	2.0532×10^{-4}
a_6	-2.69340	-2.36964
a_7	3.18540	2.81533
a_8	-1.9277×10^{-3}	2.6981×10^{-4}
a_9	-4.8174×10^{-5}	-1.1871×10^{-4}
a_{10}	3.7990×10^{-7}	7.8995×10^{-7}

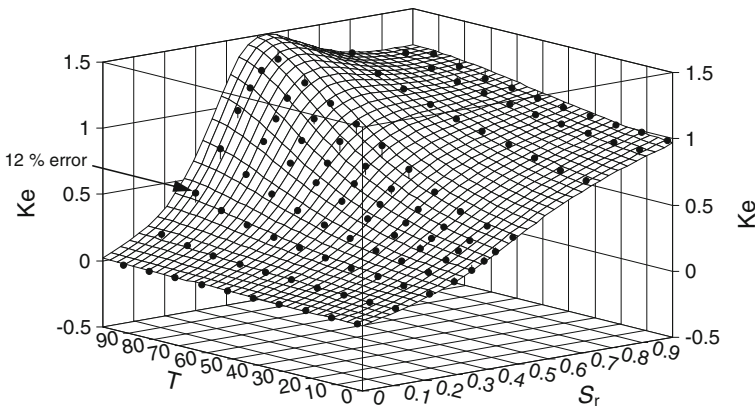


Fig. 8 Graphical representation of Eq. 16 for Ke numbers of Ottawa sand

Equation 16 is used to fit the experimental Ke numbers of Ottawa sand and Richmond Hill fine sandy loam at unfrozen states. Since most of the available soil thermal conductivity data in the literature were measured at room temperature, in order to make a Ke function easily adoptable, the thermal conductivities at dry and fully saturated states (λ_{dry} and λ_{sat}) at 22 °C are used as reference values for calculating the experimental Ke numbers of Ottawa sand and Richmond Hill fine sandy loam,

$$Ke = \frac{\lambda - \lambda_{dry@22^\circ C}}{\lambda_{sat@22^\circ C} - \lambda_{dry@22^\circ C}} \tag{17}$$

where $\lambda_{dry@22^\circ C}$ and $\lambda_{sat@22^\circ C}$ for Ottawa sand and Richmond Hill fine sandy loam are obtained from Tables 5 and 6, respectively.

The coefficients a_1 to a_{10} are obtained for each soil and remain constant for all temperatures and degree of saturations and are listed in Table 4, and the correlations are plotted along with experimental Ke values in Figs. 8 and 9, respectively.

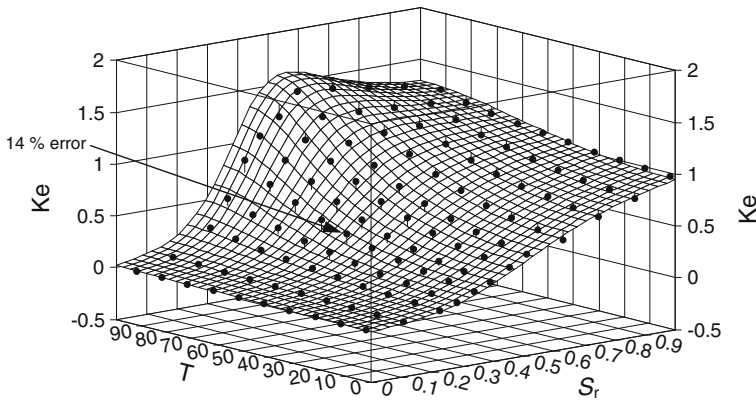


Fig. 9 Graphical representation of Eq. 16 for Ke numbers of Richmond Hill fine sandy loam

4.3 Limitations and Fitting Error of Empirical Correlation

A visual inspection indicates that the proposed empirical correlation model produces an adequate fit to the measured data for most temperatures over the saturation range considered. To assess the accuracy of the correlation quantitatively, the overall coefficients of determination, r^2 , for Ottawa sand and Richmond Hill fine sandy loam were calculated to be 0.987 and 0.976 (indicating a very good fit to the data), respectively. However, they might be slightly misleading since they were evaluated based on complete data covering all temperatures and all water contents. Thus, the high overall r^2 values in this case might not guarantee the accuracy of correlation for every temperature and water content (discrepancies can be seen in Figs. 8 and 9). In order to determine the probable error of using Eq. 16 with the coefficients in Table 4, the thermal conductivities of Ottawa sand and Richmond Hill fine sandy loam are calculated using the re-arranged Eq. 17,

$$\lambda(S_r, T) = \lambda_{\text{dry@22}^\circ\text{C}} + (\lambda_{\text{sat@22}^\circ\text{C}} - \lambda_{\text{dry@22}^\circ\text{C}}) Ke(S_r, T) \quad (18)$$

The largest individual errors between the calculated and experimental thermal conductivities for Ottawa sand and Richmond Hill fine sandy loam are calculated to be 12 % and 14 %, as indicated in Figs. 8 and 9, respectively. Meanwhile, the overall root-relative-mean-square percentage errors for Ottawa sand and Richmond Hill fine sandy loam are 4.7 % and 6.1 %, respectively, which indicates that the use of Eq. 16 is reasonable for most engineering applications.

5 Conclusions and Recommendations

Effective soil thermal conductivities of two soil types have been obtained over a wide temperature range and for full range of water content. One of the primary applications of the datasets is expected to aid the development of accurate theoretical as well as empirical high-temperature models of soil thermal conductivity. The experimental Ke

data are fitted well to an empirical correlation as a function of temperature and degree of saturation. The use of the correlation for calculating the thermal conductivities of Ottawa sand and Richmond Hill fine sandy loam gives the overall root-relative-mean-square percentage errors of 4.7 % and 6.1 %, respectively, which are reasonable for most engineering applications. It is anticipated that any existing soil thermal-conductivity model can be verified and possibly modified or recalibrated with the data to improve its accuracy. The results suggest that it would be worthwhile to extend this investigation to measure the thermal conductivity of more soil types, namely, silt, clay, loam, and peat in unfrozen as well as frozen states. Extended thermal-conductivity datasets should allow precise verification and consequently improvement to theoretical and empirical models, and may lead to a universal methodology for evaluating soil thermal conductivity.

Acknowledgments Financial support through a Research Tools and Instruments (RTI) and Discovery Grants provided by the Natural Sciences and Engineering Research Council of Canada is gratefully acknowledged. Sincerest thanks to Dr. Jasmin Schönenberger of Geological Survey of Bavaria (Germany) for providing XRD/XRF analyses of the Richmond Hill fine sandy loam and to Dr. Jinyuan Liu of the Department of Civil Engineering, Ryerson University, for using his laboratory to measure the saturated hydraulic conductivity of Ottawa sand.

Appendix

See Tables 5 and 6.

Table 5 Measured thermal conductivity ($W \cdot m^{-1} \cdot K^{-1}$) of Ottawa sand

T(°C)	$\theta_w(m^3 \cdot m^{-3})$										
	0	0.045	0.085	0.114	0.1352	0.1492	0.1631	0.183	0.27	0.333	0.366
2	0.336	0.529	0.729	0.916	1.114	1.266	1.443	1.696	2.695	3.190	3.300
12	0.338	0.536	0.766	0.992	1.200	1.367	1.547	1.806	2.800	3.220	3.329
22	0.340	0.552	0.835	1.090	1.316	1.494	1.713	1.996	2.928	3.270	3.364
32	0.343	0.568	0.890	1.190	1.477	1.701	1.954	2.287	3.090	3.340	3.416
42	0.346	0.601	0.967	1.318	1.692	1.976	2.282	2.673	3.238	3.410	3.463
52	0.350	0.630	1.051	1.471	1.954	2.300	2.655	3.059	3.382	3.490	3.537
62	0.353	0.663	1.148	1.658	2.230	2.633	3.069	3.400	3.556	3.600	3.619
72	0.357	0.713	1.282	1.900	2.528	2.989	3.449	3.722	3.759	3.724	3.689
82	0.359	0.800	1.459	2.195	2.879	3.345	3.770	4.052	3.986	3.886	3.811
92	0.363	0.920	1.725	2.632	3.440	3.904	4.248	4.446	4.292	4.078	3.956

Table 6 Measured thermal conductivity ($W \cdot m^{-1} \cdot K^{-1}$) of Richmond Hill fine sandy loam

T(°C)	$\theta_w(m^3 \cdot m^{-3})$											
	0	0.069	0.138	0.1706	0.2032	0.232	0.2684	0.302	0.3691	0.436	0.5035	0.571
2	0.221	0.240	0.285	0.349	0.435	0.503	0.620	0.737	0.816	0.998	1.126	1.301
12	0.223	0.246	0.305	0.376	0.466	0.545	0.665	0.778	0.857	1.031	1.150	1.318
22	0.225	0.253	0.328	0.410	0.511	0.594	0.720	0.835	0.914	1.080	1.186	1.332
32	0.227	0.260	0.351	0.447	0.560	0.650	0.786	0.906	0.985	1.124	1.220	1.357
42	0.229	0.268	0.376	0.492	0.624	0.726	0.880	0.997	1.071	1.180	1.278	1.388
52	0.232	0.278	0.404	0.545	0.703	0.827	0.992	1.120	1.180	1.263	1.334	1.426
62	0.234	0.289	0.433	0.598	0.793	0.955	1.139	1.271	1.327	1.368	1.402	1.447
72	0.237	0.300	0.463	0.665	0.902	1.105	1.280	1.451	1.485	1.496	1.492	1.489
82	0.239	0.312	0.511	0.744	1.034	1.263	1.447	1.658	1.650	1.624	1.594	1.546
92	0.242	0.325	0.568	0.844	1.223	1.459	1.622	1.861	1.827	1.774	1.712	1.613

References

1. B. Gangadhara Rao, D. Sing, *Can. Geotech. J.* **36**, 767 (1999)
2. B. Becker, P. Anil Misra, B. Fricke, *Int. Commun. Heat Mass Transfer* **19**, 59 (1992)
3. S. Kersten, *Thermal Properties of Soils, Bulletin 28* (Engineering Experiment Station, University of Minnesota, Minneapolis, MN, 1949)
4. A. Gemant, *Heat. Piping Air Cond.* **24**, 122 (1952)
5. O. Johansen, Ph.D. Thesis, Norwegian University of Science and Technology, Trondheim, Norway (1975)
6. D.A. de Vries, *Meded. Landbouwhoges. Wateningen* **52**, 1 (1952)
7. M. Van Rooyen, H. Winterkorn, in *Highway Research Board Proceedings*, vol. 39, 576 (1957)
8. J. Cote, J. Konrad, *Can. Geotech. J.* **42**, 443 (2005)
9. V.R. Tarnawski, W.H. Leong, *Trans. Porous Media* **41**, 137 (2000)
10. V.R. Tarnawski, F. Gori, *Int. J. Energy Res.* **26**, 143 (2002)
11. T. Farouki, *Rock Soil Mech. J.* **11**, 1 (1986)
12. A. Sepaskhah, L. Boersma, *Soil. Sci. Soc.* **43**, 439 (1979)
13. G. Campbell, J. Jungbauer Jr, W. Bidlake, R. Hungerford, *Soil Sci.* **158**, 307 (1994)
14. W. Black, R. Bush, M. Martin Jr, in *Proceedings of the 7th IEEE/PES Transmission and Distribution Conference and Exposition* (Atlanta, GA, 1979), pp. 275–280
15. Y. Hiraiwa, T. Kasubuschi, *Euro. J. Soil Sci.* **51**, 211 (2000)
16. V.R. Tarnawski, W.H. Leong, K.L. Bristow, *Int. J. Energy Res.* **24**, 1335 (2000)
17. R. Holton, O. Wirenga, D. Nielsen, *Unsat. Soil Column. Soil Sci.* **133**, 397 (1982)
18. P. Blich, C. Smith, *Apparent Thermal Conductivity Measurement of Soils in the Field and Laboratory—Using Thermal Conductivity Probe*, EEBS Report No. 25 (Solar Passive Division, U.S. Department of Energy, Washington, DC, 1983)
19. Dynatech, *The Apparent Thermal Conductivity and Thermal Resistance of Dry and Water Saturated Specimen of Ottawa Sand*, Report No. MIT-15a (Dynatech R/D Co., Cambridge, MA, 1980)
20. F. Moench, D. Evans, *Soil Sci. Soc. J.* **34**, 377 (1969)
21. K. Bristow, in *Methods of Soil Analysis: Physical Methods*, ed. by J.H. Dane, G.C. Topp. Thermal Conductivity (Soil Science Society of America, Madison, 2002), pp. 1209–1226
22. V.R. Tarnawski, M.L. McCombie, W.H. Leong, B. Wagner, T. Momose, J. Schönenberger, *Int. J. Thermophys.* **33**, 843 (2012)
23. A. Banin, A. Amiel, *Geoderma* **3**, 185 (1970)
24. I.S. Dahiya, D.J. Dahiya, M.S. Kuhad, S.P.S. Karwasra, *J. Agric. Sci.* **110**, 515 (1988)

25. D.O. Reid, I. Nikolaev, W.H. Leong, M.A. Rosen, in *Proceedings 21st Canadian Congress of Applied Mechanics*, Toronto, Canada, 2007
26. D.O. Reid, M.A. Sc. Thesis, Department of Mechanical and Industrial Engineering, Ryerson University, Toronto, 2005
27. R.J. Moffat, *Exp. Therm. Fluid Sci.* **1**, 3 (1988)
28. D.A. de Vries, in *Proceedings of the 4th International Congress of Soil Science*, vol. 70, Amsterdam, 1950, p. 38
29. V.R. Tarnawski, T. Momose, W.H. Leong, G. Bovesecchi, P. Coppa, *Int. J. Thermophys.* **30**, 949 (2009)
30. V.R. Tarnawski, T. Momose, W.H. Leong, *Int. J. Thermophys.* **32**, 984 (2011)
31. H.C. Brinkman, *Appl. Sci. Res.* **1**, 27 (1949)
32. L. Zheng, J. Samper, L. Montenegro, *J. Contamin. Hydro.* **126**, 45 (2011)
33. J.M. Sorel, *J. Contamin. Hydrol.* **53**, 63 (2001)
34. COMSOL Multiphysics 4.3, COMSOL Inc. (2012)